Localized versus Backbone Fluorescence in *N*-*p*-(Diarylboryl)phenyl-Substituted 2,7- and 3,6-Linked Polycarbazoles

Dörte Reitzenstein and Christoph Lambert*

Institut für Organische Chemie, Universität Würzburg, Am Hubland, 97074 Würzburg, Germany

Received October 6, 2008; Revised Manuscript Received December 4, 2008

ABSTRACT: The triarylborane acceptor in poly[9-((4-dimesitylboryl)-3,5-dimethylphenyl)-9*H*-carbazole]-3,6-diyl **P2** has a strong impact on the optical properties of this 3,6-linked carbazole main chain polymer and results in an enhanced fluorescence quantum yield because of a low-lying fluorescent CT state. In contrast, the same acceptor substituent does not influence the optical properties of poly[9-((4-dimesitylboryl)-3,5-dimethylphenyl)-9*H*-carbazole]-2,7-diyl **P1**. In the latter polymer, the optical properties are governed by conjugation along the carbazole backbone. This interpretation is supported by comparison with poly[9-(4-(diphenylmethyl)-phenyl)-9*H*-carbazole]-2,7-diyl **P3**, which serves as a reference polymer. Synthesis and characterization by gel permeation chromatography, NMR spectroscopy, absorption, and fluorescence measurements in solution and solid state and cyclic voltammetric measurements of the three polymers are presented.

Introduction

Owing to their promising electrical and photophysical properties,[1] polycarbazoles are interesting candidates for application in optoelectronic devices such as plastic solar cells,[2] organic field effect transistors (OFETs),[3] or organic light emitting devices (OLEDs).[4−7] Polycarbazoles are strong blue emitters with high fluorescence quantum yields,[8,9] and they are excellent hole transport materials with high thermal stability[10] and glass forming properties.[9] The 2,7-linked polycarbazoles (Chart 1A) are often favored to 3,6-linked polycarbazoles (Chart 1B) because of their higher fluorescence quantum yields in solution and their extended conjugation over several monomer units.[10,11]

This extended conjugation in poly-2,7-carbazoles results from the rigid poly-*para*-phenylene motif that is bridged by nitrogen atoms in contrast with the more flexible 1,4-diaminobiphenyl structure of poly-3,6-carbazoles that may be conceived as nitrogen-connected benzidines. However, the preparation of 3,6-disubstituted carbazoles is much easier than that of their 2,7-analogues, and 3,6-polymers are more soluble than 2,7-polymers because of the greater flexibility of the polymer backbone. Moreover, 3,6-polycarbazoles show higher in situ conductivities than their 2,7-analogues.[12]

OLEDs have been fabricated from both 2,7[6]- and 3,6-linked[4,7] polycarbazoles and from copolymers[5] containing carbazole moieties. For device efficiency, a balanced charge carrier injection and transport is important, which can be achieved by additional charge injection and charge transport layers. Bipolar molecules that contain an electron donor as well as an electron acceptor moiety can function as emission, electron, and hole transport layer at the same time. For example, triarylamines (donor, hole transport) covalently bound to triarylboranes (acceptor, electron transport) have already been successfully used in OLEDs.[13,14] Moreover, polycarbazoles closely match the hole injection energy from ITO-coated electrodes.[15] In addition, triarylboranes attached to a polymer backbone show high fluorescence quantum yields in solution and in solid state,[16,17] the latter being even more important for the application in OLEDs. The design concept of introducing boryl substituents at the lateral positions of a conjugated polymer backbone was also recently highlighted by M. Elbing and G. C. Bazan.[18]

In this work, we synthesized a 2,7- and a 3,6-linked polycarbazole with a triarylborane moiety attached to the nitrogen atom of the carbazole (**P1** and **P2**). As a reference molecule, a 2,7-linked polycarbazole with a triarylmethyl moiety attached to the nitrogen atom was used (**P3**). In this Article, we report the synthesis and some fundamental absorption and emission as well as electrochemical properties of these polymers that may be useful materials for OLED applications.

Results and Discussion

Synthesis and Characterization. The synthetic approach to monomers **6a**−**c** is outlined in Scheme 1a.

Leclerc et al. published an efficient two-step synthesis of 2,7-dichlorocarbazole **3a**.[19] However, the starting materials they used, 4-chlorophenylboronic acid and 1-bromo-4-chloro-2-nitrobenzene, are rather expensive. Therefore, we prepared **3a** in three steps starting with cheap and commercially available 1-chloro-4-iodobenzene. The first step is an Ullmann coupling reaction[20] to give 4,4′-dichlorobiphenyl **1**[21] in moderate yield, which is then nitrated to afford **2**[22] in 95% yield. Finally, a Cadogan ring closure,[23] which is also used by Leclerc et al., gives **3a**[19] in 63% yield. The 2,7- and 3,6-dichlorocarbazole **3a** and **3b**[24] are then *N*-arylated by 1,4-dibromo-3,5-dimethylbenzene **4a**[25,26] catalyzed by CuI to afford

Chart 1

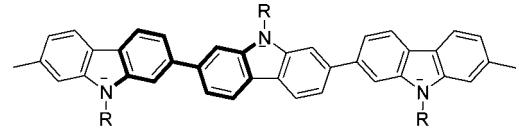

2,7-linkage (**A**)

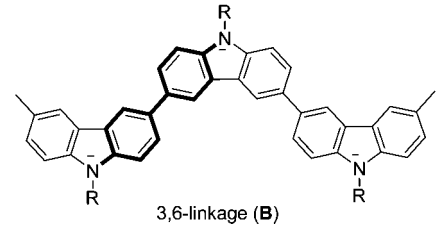

3,6-linkage (**B**)

* Corresponding author. Tel: +49-(0)931-888-5318. Fax: +49-(0)931-888-4606. E-mail: lambert@chemie.uni-wuerzburg.de.

10.1021/ma802232r CCC: $40.75
Published on Web 01/20/2009

Scheme 1. (a) Synthesis of the Monomers and (b) Polymerization

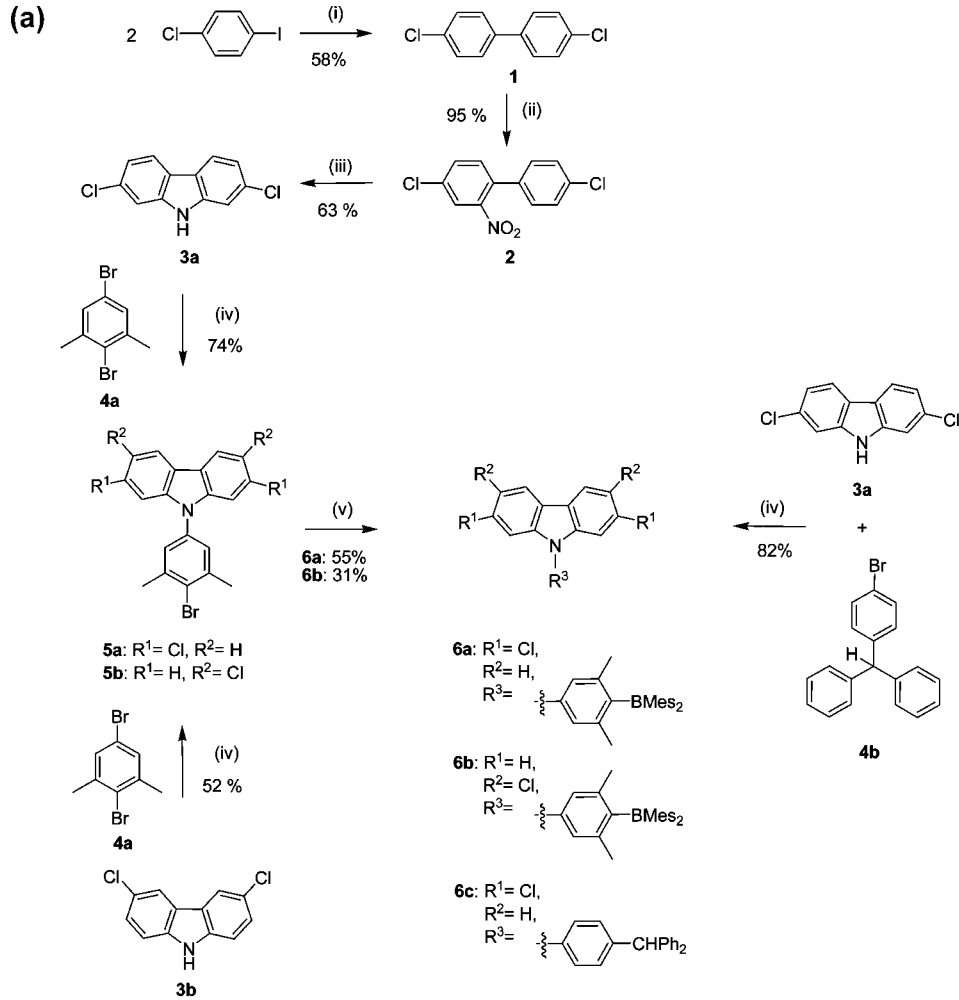

(i) Cu, 230-250 °C, 3 h; (ii) HNO_3, CH_3COOH, 110 °C, 1 h; (iii) $P(OEt)_3$, 170 °C, 16 h; (iv) CuI, K_3PO_4, *trans*-1,2-cyclohexanediamine, 1,4-dioxane, 110 °C, 72 h (19 h for **5b**); (v) 1. *t*-BuLi, Et_2O, 2. $(Mes)_2BF$, Et_2O;

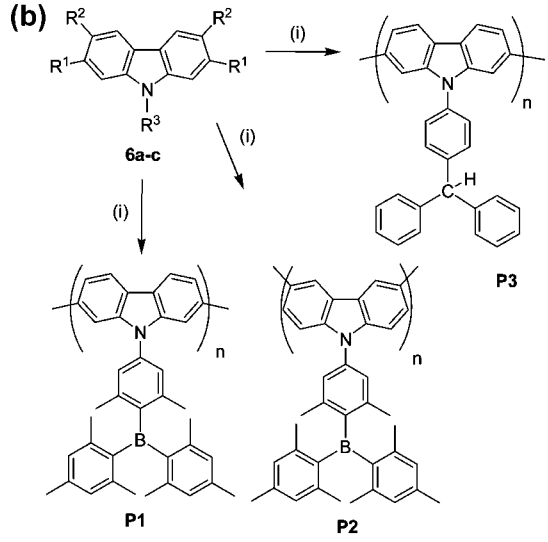

(i) Zn powder, $NiCl_2$, 2,2'-bipyridyl, PPh_3, DMAc, 70 °C, 3 d;

5a and **5b**, respectively.[27] The same reaction is applied to the attachment of 1-bromo-4-(diphenylmethyl)benzene **4b**[28] to the carbazole-nitrogen of **3a** to give the monomer **6c**. In the case of **5b**, the reaction time was only 19 h in contrast with 72 h for **5a** and **6c**, which might be the reason for the lower yield of **5b**. Finally, the reaction of dimesitylboronfluoride with the aryllithium derivatives of **5a** and **5b** affords the monomers **6a** and **6b**, respectively.[27]

Table 1. GPC Measurements in THF at 35 °C

	P1	P2	P3
M_w	2300 (4000)[a]	6000	1900
M_n	2100 (2300)	4900	1700
PDI	1.1 (1.8)	1.2	1.1
DP	4 (8)	12	5

[a] Numbers in brackets correspond to a measurement in 1,2,4-trichlorobenzene at 135 °C.

Polymerization of the monomers **6a**−**c** is achieved by the standard Yamamoto coupling reaction[29] with an in-situ-generated zerovalent nickel complex as a catalyst to give **P1**, **P2**, and **P3** (Scheme 1b) in acceptable yield (63, 53, and 52%).[19]

The 2,7-linked polymers **P1** and **P3** are only slightly soluble in chloroform, dichloromethane, and THF, whereas the 3,6-linked polymer **P2** is more soluble in these solvents because of its more flexible polymer backbone.

Gel permeation chromatography (GPC) versus polystyrene standards performed in THF at 35 °C indicated an average molecular weight, M_w, of 2300 Da (PDI = 1.1) for **P1**, 6000 Da (PDI = 1.2) for **P2**, and 1900 Da (PDI = 1.1) for **P3** corresponding to a degree of polymerization of 4, 12, and 5 monomer units, respectively (Table 1).

The higher M_w of **P2** compared with those of the 2,7-linked polymers **P1** and **P3** can possibly be attributed to the better solubility of **P2**, thus allowing the polymerization reaction to continue even for chains of higher molar mass. Moreover, it is not possible to obtain a clear solution of **P1** and **P3** in THF; that is, chains of higher molar mass might be removed by filtration before injection into the GPC columns. This explanation is substantiated by an additional GPC measurement of **P1** in trichlorobenzene at 135 °C, which gave an M_w of 4000 Da with a higher PDI of 1.8. In the latter solvent, **P1** is more soluble so that chains of higher molar mass are also injected into the GPC columns, which consequently leads to a broader molecular weight distribution. Leclerc et al.[9] reported an M_n value of 2600 Da (PDI = 1.9) for poly[*N*-(2-ethylhexyl)-2,7-carbazole] measured in THF, which corresponds to about nine repeating units. This polymer was obtained by polymerization of *N*-(2-ethylhexyl)-2,7-dichlorocarbazole via standard Yamamoto coupling with $Ni(COD)_2$ as catalyst. The same reaction method was used by Fu and Bo[30] for the polymerization of *N*-octyl-2,7-dibromocarbazole to obtain an M_n value of 6400 Da. Even higher M_n values were obtained for poly[*N*-9′-heptadecanyl-2,7-carbazole] (M_n = 27 000 Da[31]) and for poly[*N*-(2-decyltetradecyl)-2,7-carbazole] (M_n = 39100 Da[32]) using the standard Yamamoto coupling reaction. This shows that high molecular weight 2,7-linked polycarbazoles can be obtained depending on the substituent at the nitrogen atom and the exact reaction conditions. For 3,6-linked polyalkylcarbazoles a high molecular weight synthesis based on the standard Yamamoto coupling reaction was developed to yield poly[*N*-(3,7-dimethyloctyl)-3,6-carbazole] with M_w = 120 kDa using a reverse order of adding reagents.[33] To enhance the M_w values of **P1**−**P3**, one would need to optimize the reaction conditions. For example, higher dilution could avoid possible aggregation and precipitation of the resultant polymer chains.[34] However, dilute solutions of 3,6-dichlorocarbazole could promote the formation of macrocycles.[35] Lowering the reaction temperature could avoid decomposition of the Ni(II)Ar complex that would otherwise result in the termination of the polymerization process.[36] However, solubility decreases with decreasing temperature as well. Perhaps one also has to raise the $NiCl_2$/monomer ratio for small scale reactions (<1 mmol of monomer) or use $Ni(COD)_2$ instead of generating the active Ni(0) species in situ from $NiCl_2$ and Zn because $Ni(COD)_2$ is mainly used for this type of polymerization reactions in the literature. Using the dibromo instead of the dichloro monomers would certainly give better results. To this end, one has to modify the synthesis of the monomers. Using dibromo monomers would also offer the possibility of performing a Grignard metathesis polymerization initiated by Ni(II) as it is applied for the synthesis of poly(3-alkylthiophene).[34] Because optimization of the polymerization reaction was not our main goal, we did not follow any of the above-mentioned possibilities to increase the M_w values of the polymers **P1**−**P3**.

MALDI-TOF spectra revealed that not all polymer chains are terminated by hydrogen atoms. Chains of **P1** are mainly terminated by hydrogen atoms. However, there are additional small mass peaks that can be assigned to chains terminated at one end by one chlorine atom. For **P2**, only hydrogen-terminated chains are found. **P3** consists of a mixture of chains terminated by one or two chlorine atoms and chains without chlorine atoms. These findings can be an indication of the type of polymerization mechanism that takes place here: If the monomer reacts via an intermolecular catalyst-transfer condensation polymerization mechanism, then both ends of the chains should be terminated by either hydrogen or chlorine atoms. If they react via an intramolecular catalyst-transfer condensation polymerization mechanism, then one end should be terminated by a chlorine atom and the other end by a hydrogen atom.[36] Therefore, one can conclude that the polymerization of **P1** and **P2** mainly proceeds via the intermolecular mechanism, whereas the polymerization of **P3** proceeds via inter- and intramolecular catalyst-transfer condensation polymerization mechanisms. On the first sight, this is in contrast with the very narrow molecular weight distribution (PDI = 1.1 for **P1** and **P3** and 1.2 for **P2**) observed for the polymers because the intermolecular catalyst-transfer condensation polymerization mechanism is expected to result in a broader molecular weight distribution as opposed to the intramolecular mechanism.[36] However, as stated above, chains of higher molecular weight might be removed by filtration before injection into the GPC columns, and thus the real molecular weight distribution might be broader at least for **P1** and **P3**.

Nuclear Magnetic Resonance Spectra. NMR spectra of the polymers were recorded in chloroform and in THF. Although in the literature, discrete doublets and singlets are found for carbazole protons of high-molecular-weight polycarbazoles, we observed only broad signals. This is due to the short polymer chains investigated in the present work that lead to different chemical shifts for each monomer unit and, thus, to a distribution of overlapping signals. Because of their low solubility ^{13}C NMR spectra of **P1** and **P3** could not be recorded.

Absorption Spectra. Absorption spectra of 2,7-linked polymers **P1** and **P3** measured in dichloromethane are similar to each other (Figure 1) and to other 2,7-linked *N*-alkyl- and *N*-arylcarbazole polymers.[8,10,15,31] This fact nicely demonstrates that the *N*-substituents only weakly interact with the polymer backbone. Nevertheless, the absorption band of the triarylborane moiety cannot be seen because its molar extinction coefficient is too low: The absorption maximum of dimesityl(2,6-dimethylphenyl)borane dissolved in dichloromethane is at λ = 327 nm (spectrum not displayed) with ε = 13 300 $M^{-1}\cdot cm^{-1}$. The molar extinction coefficient of **P1** dissolved in dichloromethane is ca. 19 100 $M^{-1}\cdot cm^{-1}$ at λ = 327 nm.[37] Overlaying both spectra shows that the absorption band of the triarylborane compound is completely covered by the band of **P1**. The absorption edge of triphenylmethane is situated at 280 nm.[38]

Absorption spectra were also recorded for solutions of **P1** and **P3** in cyclohexane, *tert*-butyl-methyl ether (MTBE), ethylacetate, 1,4-dioxane, and THF. Only minor variations in the shape of the absorption bands with the solvent were observed, which can be explained by the fact that different solvents dissolve different weight fractions of the polymers. This interpretation is supported by the work of Iraqi et al.[10] and by

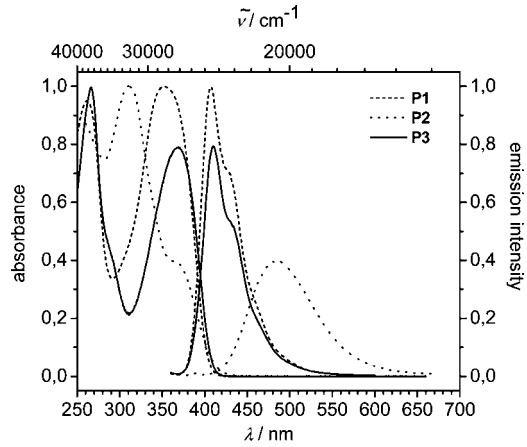

Figure 1. Absorption spectra (normalized) and emission spectra (normalized to the intensity of the lowest energy absorption band) of **P1**−**3** in dichloromethane.

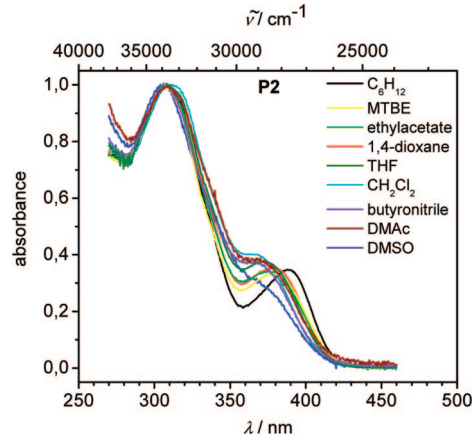

Figure 2. Normalized absorption spectra of **P2** in different solvents.

the fact that there is no systematic solvatochromism versus any solvent polarity function.

Much in contrast, the absorption spectrum of 3,6-linked polymer **P2** in dichloromethane deviates from those of the pentamer and polymer of 3,6-linked *N*-alkyl-carbazole[3] because it shows an additional low energy band at 367 nm in dichloromethane arising from a charge transfer (CT) from the carbazole donor to the triarylborane acceptor. This process causes a reversal of the dipole moment. Thus, a pronounced negative solvatochromism is observed in the absorption spectra (Figure 2), and a positive solvatochromism is found in the emission spectra of **P2** (Figure 3). This phenomenon has already been recently discussed for the monomer analogue of **P2**.[27]

Emission Spectra. Emission maxima, λ_{em}, Stokes shifts, fluorescence quantum yields, Φ_f, lifetimes, τ, and rate constants, k_f and k_{nr}, are listed in Table 2. Emission spectra of **P1** and **P3** are very similar concerning λ_{em} (407 and 410 nm in dichloromethane) and the shape of the emission bands (Figure 1). They are also very similar to other 2,7-linked *N*-alkyl and *N*-aryl-carbazole polymers reported in the literature.[8−10] The Stokes shifts are somewhat higher in energy than that of already known 2,7-polycarbazoles (poly[*N*-(2-ethylhexyl)-2,7-carbazole]: 2300 cm^{-1})[39] with that of **P1** being also higher than that of **P3** (3800 vs 2800 cm^{-1}). In going from cyclohexane to dichloromethane, both polymers show small solvatochromic shifts of about 400 (**P1**) and 700 cm^{-1} (**P3**). Therefore, fluorescence quantum yields, Φ_f, and lifetimes, τ, were measured in dichloromethane only. Rate constants, k_f and k_{nr}, are calculated according to eqs 3 and 4, which can be derived from combination of eqs 1 and 2

$$\tau = \frac{1}{k_f + k_{nr}} \quad (1)$$

$$\Phi_f = \frac{k_f}{k_f + k_{nr}} \quad (2)$$

$$k_f = \frac{\Phi_f}{\tau} \quad (3)$$

$$k_{nr} = \frac{1 - \Phi_f}{\tau} \quad (4)$$

The k_f and k_{nr} values of **P1** are about half of those of poly[*N*-octyl-2,7-carbazole] ($k_f = 17 \times 10^8$ s^{-1}; $k_{nr} = 4.3 \times 10^8$ s^{-1}, $\tau = 0.48$ ns, $\Phi_f = 0.80$), whereas the lifetime is doubled and the quantum yield is the same.[39] The Φ_f, τ, k_f, and k_{nr} values of **P3** are similar to the corresponding values of **P1** (Table 2). All of these similarities of **P1** and **P3** and other 2,7-linked polycarbazoles and the lack of solvatochromic fluorescence of **P1** clearly show that the triarylborane substituent does not influence the fluorescence properties in this type of polymer. Thus, one can conclude that fluorescence in **P1** and **P3** emanates from the polymer backbone.

Unlike **P1** and **P3**, **P2** shows strong solvatochromic fluorescence arising from a low-lying CT state. The energy shift between the emission maxima in cyclohexane and DMSO is 3800 cm^{-1}. In Table 3, emission maxima, λ_{em}, Stokes shifts, quantum yields, Φ_f, lifetimes, τ, and rate constants, k_f and k_{nr}, are listed for solvents of increasing polarity.

Except for the values obtained in 1,4-dioxane, emission maxima, band widths and Stokes shifts increase with increasing solvent polarity as expected for CT transitions. Whereas the lifetimes of the CT state increase with decreasing fluorescence energy, the quantum yields do not reveal a clear trend. As expected from the Strickler−Berg equation,[40] k_f should be proportional to the cubic fluorescence energy. Whereas this is not exactly fulfilled with the present data set, at least an increase in k_f with the fluorescence energy is clearly visible. According to the gap rule of Siebrand,[41] the nonradiative rate constant, k_{nr}, should increase with decreasing fluorescence energy. However, the opposite trend is observed. This unusual trend together with the same solvatochromic shifts and somewhat

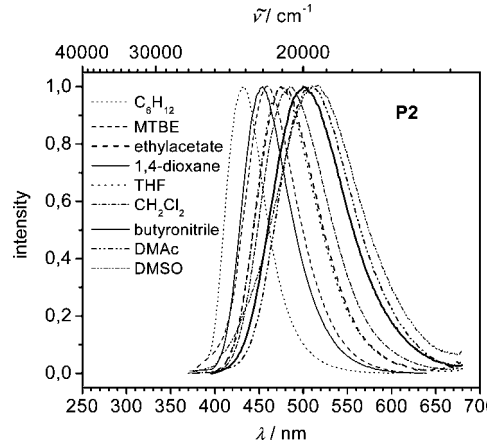

Figure 3. Normalized emission spectra of **P2** in different solvents.

Table 2. Absorption and Emission Maxima, λ_{abs} and λ_{em}, Fluorescence Quantum Yields, Φ_f, Lifetimes, τ, and Rate Constants, k_f and k_{nr}, Measured in Dichloromethane

	λ_{abs}/ nm	λ_{em}/ nm	stokes shift/cm^{-1}	Φ_f	τ/ ns	k_f/ 10^8 s^{-1}	k_{nr}/ 10^8 s^{-1}
P1	261, 353	407	3800	0.80	0.96	8.3	2.1
P2	257, 310, 365	484	6700	0.54	8.5	0.64	0.54
P3	267, 369	410	2800	0.85	0.77	11	1.9

smaller Stokes shifts have also been observed for the monomer analogue,[27] but an explanation of the violation of Siebrand's gap rule is still missing. In comparison with the monomer, lifetimes of **P2** are about twice as high and k_f values are about one-third of the values of the monomer, whereas k_{nr} values are the same for monomer and polymer. Therefore, the quantum yields of the polymer are lower than those of the monomer. Thus, counterintuitively, it is not any additional nonradiative pathway that leads to the decreased fluorescence quantum yield of the polymer compared with the monomer but the smaller fluorescence rate constant.

Compared with the emission spectra of 3,6-linked *N*-alkylcarbazole polymers, which emit at $\lambda_{em} = 426$ nm in dichloromethane,[42] the emission band of **P2** is much broader and is shifted to lower energy ($\lambda_{em} = 484$ nm in dichloromethane) because of its low-lying CT state. The Stokes shift of 6700 cm^{-1} in dichloromethane is somewhat smaller than that of *N*-alkyl-3,6-carbazole polymers.[33,35,42] Interestingly, fluorescence quantum yields are surprisingly high compared for example with poly-[*N*-decyl-3,6-carbazole] with $\Phi_f = 0.15$ in THF[33] and other 3,6-linked *N*-alkylcarbazole polymers with $\Phi_f = 0.04$ to 0.06 in dichloromethane.[42] The reason for the enhanced quantum yield obviously is the CT character of the fluorescing state, although the quantum yield is still somewhat lower than that of **P1** and **P3**. The improved quantum yield compared with *N*-alkyl-3,6-carbazole polymers makes **P2** a promising candidate as a light-emitting as well as a hole and electron transporting polymer for application in OLEDs.

The most interesting aspect about **P1** and **P2** is their absorption and emission properties being completely different (Figure 1). The fact that **P1** has a higher fluorescence quantum yield than **P2** was to be expected on the basis of the properties of other poly-*N*-alkyl-carbazoles. The higher k_f value compared with the k_{nr} value of **P1** is in accordance with its higher quantum yield. However, polymer **P2** shows negative solvatochromic absorption and positive solvatochromic fluorescence resulting from a low-lying CT state. Because the same characteristics are found, for the monomer analogue,[27] we conclude that the fluorescent CT state in **P2** is localized within the monomer site. Much in contrast, no solvatochromic behavior is observed for **P1** that fluoresces from a delocalized state of the polymer backbone. This is because **P1** forms a true conjugated (poly-*para*-phenylene type) polymer with low-lying delocalized states, whereas **P2** is a polybenzidine with conjugation being interrupted by the nitrogen atoms. Thus, the state located at the polymer backbone will be high-lying in **P2** compared with the localized CT state (Figure 4).

Whereas no pronounced solvent effect was visible in **P1**, a solvent effect was observed for a 2,7-linked polycarbazole substituted by 4-dioctylamino-benzene at the nitrogen atom, which shows dual fluorescence in polar solvents.[15] The dual fluorescence possibly arises from a fluorescent delocalized state of the polymer backbone and from a fluorescent intramolecular CT state between the dioctylaminophenyl substituent and the carbazole moiety. Interestingly, the emission maximum of the supposed CT emission band and the Stokes shifts between the absorption maximum and the CT emission band in THF and dichloromethane are quite close to those observed for **P2** in these solvents. In the case of **P1**, such a CT state might be higher in energy than the delocalized state of the polymer backbone. Thus no solvent effect is observed for the fluorescence of **P1**.

Table 3. Emission Maxima, λ_{em}, Fluorescence Quantum Yields, Φ_f, Lifetimes, τ, and Rate Constants, k_f and k_{nr}, of P2 Measured in Different Solvents

solvent	λ_{em}/nm	stokes shift/cm^{-1}	Φ_f	τ/ns	$k_f/10^8$ s^{-1}	$k_{nr}/10^8$ s^{-1}
cyclohexane	432	2700	0.37	3.2	1.2	2.0
MTBE	459	4700	0.48	5.3	0.91	0.98
ethylacetate	475	5900	0.44	6.4	0.69	0.88
1,4-dioxane	453	4500	0.62	5.3	1.2	0.72
THF	475	5900	0.54	7.3	0.74	0.63
dichloromethane	484	6700	0.54	8.5	0.64	0.54
butyronitrile	501	7500	0.40	9.9	0.40	0.61
DMAc	509	7800	0.51	13	0.39	0.38
DMSO	514	8100	0.75			

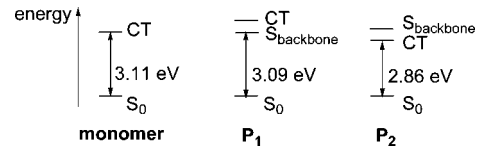

Figure 4. Qualitative energy diagram of ground and excited electronic states of **P1**, **P2**, and their monomer analogue. Gap energies are taken from the onsets of the absorption spectra of cyclohexane solutions.

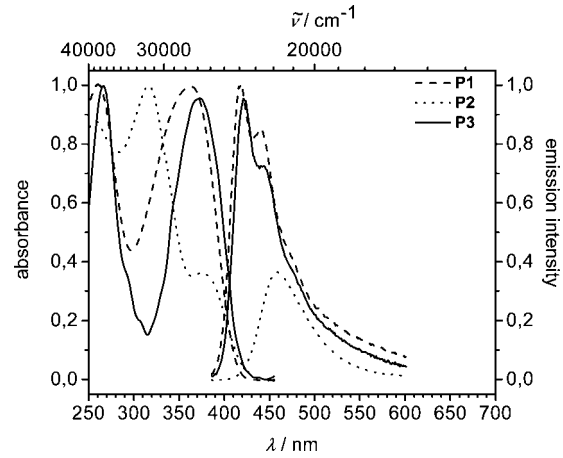

Figure 5. Absorption spectra (normalized) and emission spectra (normalized to the intensity of the lowest energy absorption band) of thin films of **P1**−**3**.

Table 4. Absorption and Emission Maxima, λ_{abs} and λ_{em}, and Fluorescence Quantum Yields, Φ_f, of Powders and Films

	λ_{abs}(film)/nm	λ_{em}(film)/nm	E_g^{opt}/eV	Φ_f(powder)	Φ_f(film)
P1	260, 363	418	2.92	0.21	0.09
P2	316,379	461	2.81	0.28	0.15
P3	266, 373	422	2.86	0.23	0.25

Absorption and emission bands recorded of thin films of the polymers cast on quartz plates are slightly red-shifted except for the solid-state emission of **P2**, which reveals an emission maximum of $\lambda_{em} = 461$ nm, which is similar to the one in MTBE (459 nm) (Figure 5, Tables 3 and 4). This indicates that the polymer itself provides a relatively apolar environment. In general, the fluorescence signals are not much broader in the solid state than in solution, which is also favorable for OLED applications. Optical band gaps, E_g^{opt}, determined from the onsets of the absorption bands are 2.92, 2.81, and 2.86 eV for **P1**, **P2**, and **P3**. These values fit well in the range of 2.89 to 3.2 eV observed for other 2,7-linked polycarbazoles depending on the conjugation length.[9,11,15,31,32] In contrast, the bandgap of **P2** is exceptionally small compared with that of other 3,6-linked polycarbazoles that have E_g^{opt} values of about 3.2 eV.[11,43,44] This is again due to the low-lying CT state.

Emission quantum yield measurements of powders of **P1**, **P2**, and **P3** gave values of 0.21, 0.28, and 0.23, respectively, whereas quantum yields of the films (drop cast) were 0.09, 0.15, and 0.25 (Table 4). The latter values depend on the film quality and might be different for spin-coated films. Nevertheless, solid-state quantum efficiencies between 0.20 and 0.30 are reasonably high compared with other solid-state quantum efficiencies of conjugated carbazole polymers.[15]

Table 5. Oxidation and Reduction Potentials versus. Fc/Fc^+ of P1, P2, and P3

	solvent	E_{ox}^1/V	E_{ox}^2/V	E_{ox}^3/V	E_{red}^1/V
P1	MeCN	+0.58[a]	+0.83[a]	+1.02[b]	−2.51[a]
P2	MeCN	+0.53[a]	+0.83[a]		−2.49[a]
	THF				−2.49[a]
P3	MeCN	+0.60[a]	+0.84[a]	+0.96[c]	−2.40[b]

[a] Half-wave potential, $v = 100$ mV·s^{-1}. [b] Peak potential, chemically irreversible, $v = 2$ V·s^{-1}. [c] Peak potential, chemically irreversible, $v = 100$ mV·s^{-1}.

Table 6. HOMO, LUMO, and Electrochemical Band Gap Energies, E_g, of P1, P2, and P3 versus Vacuum[a]

	solvent	HOMO/ eV	LUMO/ eV	E_g/ eV	HOMO/ eV[d]	LUMO/ eV[d]	E_g/ eV
P1	MeCN	−5.43[b]	−2.42[b]	−3.01	−5.15	−2.52	2.63
P2	MeCN				−5.04	−2.54	2.50
P3	MeCN	−5.45[c]			−5.20		

[a] On the basis that Fc/Fc^+ is 4.8 eV below the vacuum level. [b] From onset of the first reversible oxidation (HOMO)/reduction (LUMO) potential of non-cross-linked **P1** ($v = 2$ V·s^{-1}). [c] From onset of the first reversible oxidation potential (HOMO) of non-cross-linked **P3** ($v = 100$ mV·s^{-1}). [d] From onset of the first reversible oxidation (HOMO)/reduction (LUMO) potential of **P2** and of cross-linked **P1** and **P3** ($v = 100$ mV·s^{-1}).

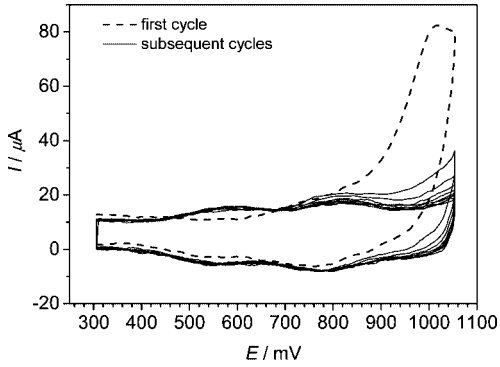

Figure 6. Multisweep CV of **P1** drop cast onto a Pt-working electrode in MeCN/TBAP (0.1 M), $v = 2$ V·s^{-1}.

Cyclic Voltammetric Measurements. Cyclic voltammetric (CV) measurements were carried out in acetonitrile/tetrabutylammonium perchlorate (TBAP) with the polymer being drop cast onto a Pt-working electrode from a dichloromethane solution. Results are listed in Tables 5 and 6.

Polymers **P1** and **P3** are oxidized at $E_{pa} = +1.02$ and +0.96 V, respectively. This process is chemically irreversible for both polymers. Upon back reduction, two new signals appear ($E_{1/2} = +0.58$ and +0.83 V for **P1** and $E_{1/2} = +0.60$ and +0.84 V for **P3**), which are reversible upon multisweep oxidation at high scan rates of 2 V·s^{-1}. At lower scan rates (100 mV·s^{-1}), the signals of **P1** drop because of detachment of the polymer from the electrode surface during the measurement. The irreversible oxidation signal disappears after the first redox cycle for both polymers. The new signals arise from CC bond formation between polymer chains at 3,6-position, which leads to benzidine units that can typically be oxidized twice.[10,12] A multisweep CV of the oxidation processes of **P1** is displayed in Figure 6, which is qualitatively similar to that of **P3**.

Two reversible oxidation signals similar to the reversible oxidation signals of **P1** and **P3** are also observed for **P2** ($E_{1/2} = +0.53$ V and +0.83 V), where the benzidine units are already present in the polymer backbone (Figure 7). The reduction of **P2** is at $E_{1/2} = -2.49$ V. However, the back oxidation peak is much smaller than the reduction peak, and both peaks drop from one cycle to the next because of dissolution of the negatively charged polymer. Therefore, a CV of **P2** dissolved in THF/TBAP was additionally recorded. This CV shows a fully reversible signal at $E_{1/2} = -2.49$ V.

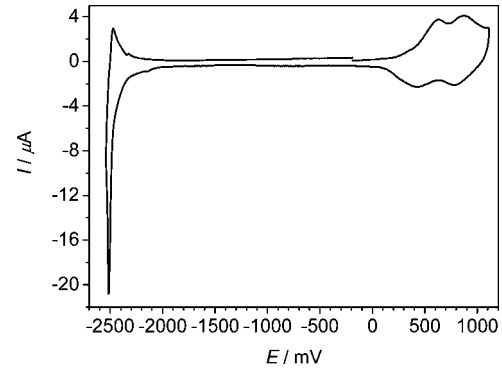

Figure 7. CV of **P2** drop cast onto a Pt-working electrode in MeCN/TBAP (0.1 M), $v = 100$ mV·s^{-1}.

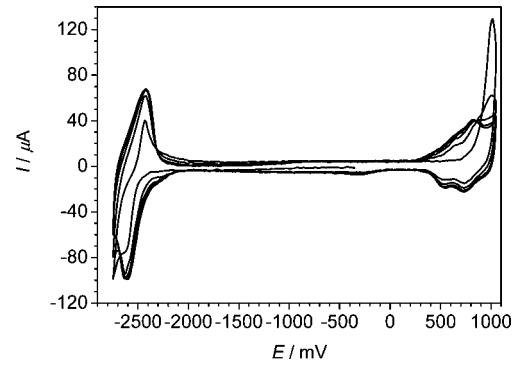

Figure 8. Multisweep CV of **P1** drop cast onto a Pt-working electrode in MeCN/TBAP (0.1 M), $v = 2$ V·s^{-1}, first cycle: reduction and oxidation before cross-linking.

The reduction of **P1** is chemically reversible only if the polymer film is previously cross-linked, which renders the polymer film insoluble avoiding its detachment from the electrode surface. Before cross-linking, the reduction takes place at $E_{1/2} = -2.53$ V determined at a scan rate of $v = 2$ V·s^{-1}. At a lower scan rate, this peak is difficult to observe. At this high scan rate, the peak separation between the reduction and the back oxidation peak is about 200 mV, which indicates a slow electron transfer between electrode surface and polymer film. After cross-linking, $E_{1/2} = -2.51$ V and the signal becomes broader and more intense (Figure 8).

A CV of **P1** recorded at $v = 100$ mV·s^{-1} after cross-linking shows a peak separation of about 80 mV and irreversible signals at $E_{pc} = -2.14$ V and at $E_{pa} = +0.33$ V (Figure 9) that are not observed if multisweep scans are exclusively run in one potential range (either between 0 mV and −2.80 V or between 0 mV and +1.10 V). These signals are more intense at scan rates of $v = 100$ mV·s^{-1} than at $v = 2$ V·s^{-1} (Figure 5). Their origin is presently unclear.

No reduction process is observed for **P3** if the polymer film is not previously cross-linked. After cross-linking, only an irreversible signal is observed at $E_{pc} = -2.38$ V that is not recovered in the following cycles, whereas the oxidation signals appear unchanged (Figure 10). It might result from an adduct being formed during the first oxidation of the 2,7-linked carbazole backbone. Similar to **P1**, there are irreversible signals at $E_{pc} = -2.14$ V and at $E_{pa} = +0.34$ V that are very small if multisweep scans are exclusively run in one potential range.

Because no reversible reduction process is observed for **P3**, whereas reversible reductions in the same potential region as those of **P1** and **P2** are observed for dimesityl(2,6-dimethylphenyl)borane ($E_{1/2} = -2.59$ V vs Fc/Fc^+, 0.7 mM in THF/TBAP

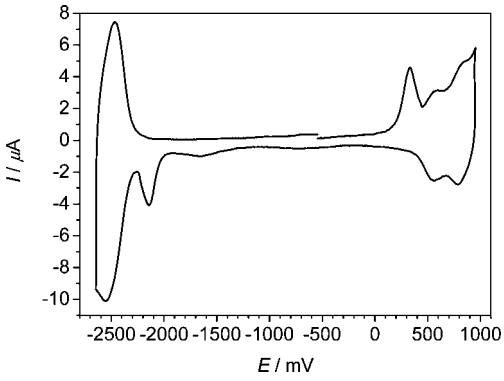

Figure 9. CV of **P1** drop cast onto a Pt-working electrode in MeCN/TBAP (0.1 M), $v = 100$ mV·s^{-1}, recorded after interchain coupling, second cycle of an oxidation−reduction-multisweep CV.

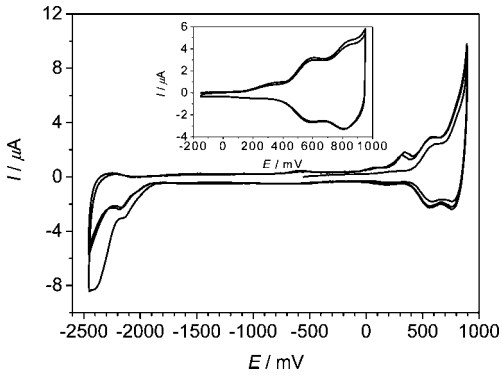

Figure 10. Multisweep CV of **P3** drop cast onto a Pt-working electrode in MeCN/TBAP (0.1 M), $v = 100$ mV·s^{-1}, recorded after interchain-coupling; inset: two oxidation cycles.

0.3 M, $v = 250$ mV·s^{-1}, Pt-working electrode) and for the monomer analogue ($E_{1/2} = -2.48$ V vs Fc/Fc$^+$, 0.6 mM in THF/TBAP 0.3 M, $v = 100$ mV·s^{-1}, Pt-working electrode), the reduction process of **P1** and **P2**, respectively, should be localized at the borane moiety. The reduction in the carbazole moiety is not seen for any of the three polymers, which seems to be the case for most polycarbazoles in the literature.[31] Only Zotti and coworker[12] reported the reduction of poly(*N*-octyl-2,7-carbazolediyl) at $E°_{red} = -2.68$ V versus Ag/0.1 M $AgClO_4$ in acetonitrile, and Iraqi and coworker[45] found, a reduction potential of $E°_{red} = -2.1$ V versus Ag/$AgNO_3$ for a drop cast polymer film of 3,6-nitrile-substituted polycarbazole.

HOMO and LUMO energies determined from the onset of the first reversible oxidation and reduction processes of **P2** and of the non-cross-linked and cross-linked polymers **P1** and **P3** and the corresponding energy band gaps, E_g, are listed in Table 6. The HOMO energies of **P1** and **P3** are −5.43 and −5.45 eV, respectively. HOMO energies of other 2,7-linked polycarbazoles are at −5.99,[31] −5.6,[32] and −5.4 eV.[10] Cross-linking raises the HOMO levels of **P1** and **P3**, which results in quite similar HOMO energies for all three polymers (−5.15 (**P1**), −5.04 (**P2**), and −5.20 eV (**P3**)) that, thus, lie in the range of those of 3,6-linked polycarbazoles (−5.0[43] and −5.1 eV[42]). The lowering of the HOMO energies can be explained by the donating abilities of the nitrogen atoms arranged para to each other after cross-linking. The LUMO energy of **P1** is also lowered from −2.42 eV before cross-linking to −2.52 eV after cross-linking, which has to do with the broadening of the peak after cross-linking and results in a value similar to that of **P2** (−2.54 eV). However, note that the half-wave potentials of the reduction of **P2** and of non-cross-linked and cross-linked **P1** are all more or less the same, which means, that the reduction is not much affected by the type of carbazole connection and is

Figure 11. Lateral and top view of a single layer OLED of **P2**.

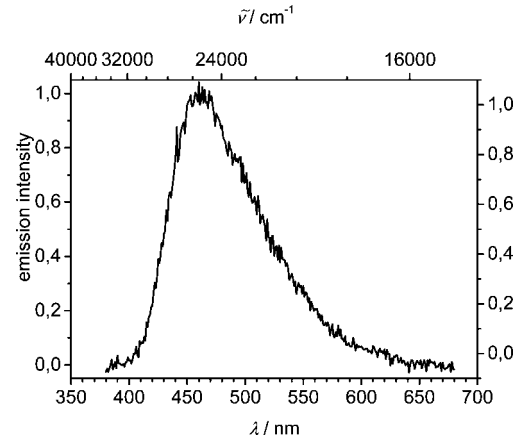

Figure 12. Electroluminescence spectrum of the device ITO/**P2**/Al.

located at the borane moiety. The LUMO energy of **P3** could not be determined because the origin of the irreversible reduction signal after cross-linking is unclear and might result from an adduct. Accordingly, the electrochemical band gap energy, E_g, of **P3** calculated as the difference between HOMO and LUMO energy could not be determined.[46] The band gap energies for non-cross-linked **P1**, for cross-linked **P1**, and for **P2** are $E_g =$ 3.01, 2.63, and 2.50 eV, respectively.

Absorption spectra of polymer films of **P1** and **P3** on a Pt-working electrode in MeCN/TBAP before and after cross-linking were additionally recorded and clearly show the narrowing of E_g upon cross-linking. Unfortunately, the spectra were of a rather poor quality so that quantitative information like optical band gap energies and shifts in absorption maxima could not be derived.

Single-Layer Organic Light Emitting Device. A single-layer OLED was constructed with **P2** to prove its electroluminescent properties. A solution of **P2** in chloroform/toluene (25:1; 6 mg/mL) was spin coated onto ITO-coated glass plates (2.5 × 2.5 cm^2), and Al contacts (90 nm) were deposited on top, as illustrated in Figure 11. The electroluminescence spectrum was recorded at an applied voltage of 8.5 V (Figure 12). The emission maximum was at $\lambda = 463$ nm, which is only a 2 nm red shift compared with that of the photoluminescence spectrum of the polymer film (Table 4). The Commission International d'Eclairagee (CIE) coordinates are (0.17, 0.21). R. Liu and coworkers got CIE coordinates of (0.17, 0.14)[47] for a single-layer OLED of 2,7-fluorene-*co*-3,9-carbazole copolymer, which indicates a more saturated color. Electroluminescence spectra of **P1** and **P3** could not be reproducibly recorded. This is possibly caused by their low solubility, which results in very thin polymer layers.

Conclusions

Poly[9-((4-dimesitylboryl)-3,5-dimethylphenyl)-9*H*-carbazole]-2,7-diyl **P1**, poly[9-((4-dimesitylboryl)-3,5-dimethylphenyl)-9*H*-carbazole]-3,6-diyl **P2**, and poly[9-(4-(diphenylmethyl)-phenyl)-9*H*-carbazole]-2,7-diyl **P3** have been synthesized by the Yamamoto coupling reaction. We found, that the triarylborane substituent in 2,7-linked polymer **P1** does not have any influence on absorption and emission properties, which is evident by

comparison with the reference polymer **P3** and with other known 2,7-linked polyalkylcarbazoles. This is possibly due to effective conjugation along the polymer backbone, which results in a polymer state being lower in energy than an intramolecular CT state involving the boron and nitrogen centers. However, the triarylborane substituent in 3,6-linked polymer **P2** has a pronounced influence on the optical properties of **P2**: a low energy CT-absorption band and an emission maximum that is also lower in energy than those of known 3,6-linked polyalkylcarbazoles are observed. This is because conjugation along the polymer backbone is interrupted by the nitrogen atoms, which makes the intramolecular CT state the lowest electronically excited state. Measurements in different solvents revealed negative solvatochromic absorption and positive solvatochromic emission. Fluorescence quantum efficiencies of **P2** are fairly high even in solid state, which we attribute to the existence of the low-lying CT state. Violation of Siebrand's rule leads in effect to a high fluorescence quantum yield for **P2** irrespective of the solvent polarity. Altogether, absorption and emission properties of **P2** are similar to the corresponding monomer, whereas absorption and emission properties of **P1** and **P3** are similar to 2,7-linked polyalkylcarbazoles.

CV measurements showed that end groups of 2,7-linked polymers **P1** and **P3** couple in 3,6-position upon oxidation, resulting in two new reversible oxidations of the cross-linked polymer similar to the two reversible oxidation peaks of 3,6-linked polymer **P2**. Before and after cross-linking of **P1** and for **P2**, one reversible reduction process at $E_{1/2} = -2.53$ and -2.51 V (**P1**) and $E_{1/2} = -2.49$ V (**P2**) located at the borane moiety is observed, whereas for cross-linked **P3**, one irreversible reduction at $E_{pc} = -2.38$ V is observed, which might arise from an adduct being formed during oxidation. Cross-linking raises the HOMO levels of **P1** and **P3** up to the range where the HOMO energies of 3,6-linked polycarbazoles lie, whereas the LUMO energy of **P1** is not much affected by cross-linking.

P2 seems to be a promising candidate for the application in OLEDs. It has an average degree of polymerization of 12 monomer units, it is soluble in common organic solvents, it consists of hole and electron transporting moieties, and it is a blue emitter with CIE coordinates of (0.17, 0.21) and a reasonably high quantum yield in solution and in solid state.

Experimental Section

Materials. All reactions were carried out under nitrogen atmosphere using standard Schlenk techniques. THF and diethyl ether were distilled over sodium/benzophenone, and 1,4-dioxane was distilled over sodium. All other chemicals and reagents were used as received. Synthesis of 4,4'-dichlorobiphenyl **1**,[21] 4,4'-dichloro-2-nitrobiphenyl **2**,[22] 2,7-dichlorocarbazole **3a**,[19] 3,6-dichlorocarbazole **3b**,[24] 1,4-dibromo-3,5-dimethylbenzene **4a**,[25,26] and 1-bromo-4-(diphenylmethyl)-benzene **4b**[28] have already been reported in the literature.

Characterization. ^{1}H and ^{13}C NMR spectra were recorded with either a Bruker AVANCE 400 FT-NMR spectrometer or a Bruker AVANCE DMX 600 FT-NMR spectrometer at room temperature. Tetramethylsilane was used as an internal standard.

Mass spectra were recorded with a Finnigan MAT 90 and with a Bruker Daltonics micrOTOF focus mass spectrometer equipped with an APCI ion source (Agilent G1947−60101). Mass spectra of the polymers were recorded with a Bruker Daltonik autoflex II with samples being embedded in a DCTB matrix [$(H_3C)_3C$-*p*-Ph-CH=C(CH_3)-*trans*-CH=C($CN)_2$].

Number-average (M_n) and weight-average (M_w) molecular weights were determined by GPC with a dual-plunger, tandem-flow pump (Shimadzu, LC-10AT), a He-degasser unit (Shimadzu, DGU-10B), three SDV columns from PSS/Mainz (Germany) (pore size: 100, 10^3, and 10^5 Å; particle size: 5 μm; column length: 300 mm each) and a Gynkotek model 160 UV detector. The eluent was THF (Acros, HPLC grade) at 35 °C with a flow rate of 1 mL/min. The calibration curve was made with a series of monodisperse polystyrene standards (PSS/Mainz, Germany; concentration: 1 mg/mL).

Elemental analysis was done with a Vario Micro Cube instrument (Elementar).

Ultraviolet/Visible Absorption. UV/vis absorption spectra were recorded on a JASCO V-570 UV/vis/NIR spectrometer in 1 cm quartz cells (Hellma) at room temperature. All solvents were of spectroscopic grade and used as received. For solid-state absorption spectra, we prepared thin films by spin coating dichloromethane solutions of the polymers onto quartz plates.

Steady-State Fluorescence. Steady-state fluorescence spectra were recorded on a PTI (Photon Technology International) fluorescence spectrometer model QM-2000-4 with a cooled photomultiplier (R928 P) and a 75 W xenon short arc lamp (UXL-75XE, Ushio). All spectra were recorded in 1 cm quartz cells in solvents of spectroscopic grade at room temperature. The fluorescence quantum yields were determined from the absorption and fluorescence spectra according to eq 5, in which $I(\tilde{\nu})$, OD, and n_D^{20} denote the area below the emission band, the optical density of the solution at the excitation wavelength, and the refractive index of the solvent, respectively.

$$\Phi_f = \Phi_{f,ref}\left(\frac{I(\tilde{\nu})(OD_{ref})(n_D^{20})^2}{I(\tilde{\nu})_{ref}(OD)(n_{D,ref}^{20})^2}\right) \quad (5)$$

Quinine sulfate dihydrate (Fluka) in 1 N sulfuric acid (Acros) was employed as a fluorescence standard ($\Phi_{f,ref} = 0.546$, $n_D^{20} = 1.3445$).[48] For absorption measurements, ODs were in the range of 0.01 to 0.045 to get sufficiently high signal-to-noise ratios. For emission measurements, samples were diluted by a factor of 1:10 because at higher concentrations, fluorescence quantum yields are quenched. To avoid mistakes arising from dilution, three samples per solvent were prepared. For each sample, its absorption spectrum was recorded, it was diluted, and its emission spectrum was recorded. The OD of the quinine sulfate dihydrate solution was about 0.01 and was not altered before the emission measurement. Samples were not degassed, thus avoiding concentration variations of solutions prepared from volatile solvents. Moreover, fluorescence quantum yields of polymers diluted in DMSO are only slightly higher when degassed by bubbling argon through the cuvette than those of samples not treated with an argon gas flow. Samples were excited at $\lambda = 340$, 345, and 350 nm which gave similar values for all three wavelengths for **P1** and **P3** and slightly differing values for the three wavelengths for **P2**. Results are only tabulated for $\lambda = 345$ nm excitation. Solid-state emission spectra were recorded on thin films prepared by dropping dichloromethane solutions of the polymers onto quartz plates. Solid-state fluorescence quantum yields were determined on a Hamamatsu Absolute PL quantum yield measurement system CC9920−02. The system is made up of an excitation source that uses a 150 W CW xenon light source, a monochromator (250−700 nm, fwhm 10 nm), an integrating sphere, and a multichannel spectrometer capable of simultaneously measuring multiple wavelengths between 300 and 950 nm and counting the number of absorbed and emitted photons. With this system, the absolute fluorescence quantum yield of powders and thin films (drop cast, see above) was determined at room temperature on air upon excitation at $\lambda = 345$ nm.

Time-Dependent Fluorescence-Decay. Time-dependent fluorescence−decay measurements were performed with a PTI TM-2/2003 fluorescence-lifetime spectrometer with a nanosecond flash lamp charged with H_2/N_2 (1:1) at room temperature. We determined the instrument response of the nanosecond flash lamp by using colloidal silica (Ludox) in deionized water as a scatterer. The fluorescence−decay curves were fitted with a single-exponential decay function to obtain the corresponding fluorescence lifetimes.

Cyclic Voltammetry. CV experiments were carried out under an argon atmosphere with 0.1 to 0.3 M TBAP (*Caution: Organic perchlorates are potentially explosive!*) as the supporting electrolyte. Acetonitrile (Baker, HPLC grade) was predried over molecular sieve (3 Å) and distilled over CaH_2. THF was distilled over sodium/

benzophenone. A conventional three-electrode setup consisting of a platinum-disk working electrode (2 mm in diameter), an Ag/AgCl pseudoreference electrode, and a platinum-wire counter electrode was used. The redox potentials were referenced against the ferrocene/ferrocenium redox couple as an internal standard. For thin film measurements, a solution of the polymer in dichloromethane was drop cast onto the working electrode and dried under a nitrogen gas flow.

Single-Layer Organic Light Emitting Device. An ITO-coated glass plate (2.5 × 2.5 cm^2, 125 nm, sheet resistance ∼25 Ω, Merck KGaA) was covered with tape except for a bar of ∼0.5 cm width. This bar was treated with a Zn/H_2O suspension and HCl to remove ITO from the glass plate. The plate was mechanically cleaned with dish liquid and then with acetone and isopropanol in an ultrasonic bath. **P2** dissolved in chloroform/toluene (25:1, 6 mg/mL) was spin coated onto the plate. Opposite to the bar of pure glass, a bar of the polymer layer was scratched off. On top, Al contacts (90 nm, Mateck GmbH) were deposited by thermal evaporation at high vacuum (1×10^{-6} mbar, deposition rate 0.2 nm s^{-1}) in a BOC Edwards Auto 306/500 deposition system. Voltage was applied by the electrochemical workstation BAS CV-50 W. Spectra were recorded on a PTI fluorescence spectrometer model QM-2000-4 with a cooled photomultiplier (R928 P).

Preparation of Monomers. *9-(4-Bromo-3,5-dimethylphenyl)-2,-7-dichloro-9H-carbazole* **5a**.[27] **3a** (8.31 g, 35.2 mmol), **4a** (5.57 g, 21.1 mmol), CuI (224 mg, 1.18 mmol), *trans*-1,2-cyclohexanediamine (290 μL, 2.41 mmol), and K_3PO_4 (15.7 g, 74.0 mmol) were suspended in dry 1,4-dioxane (22 mL) and heated to 110 °C for 72 h. The reaction mixture was diluted in dichloromethane and washed with water. The combined aqueous phases were extracted with dichloromethane, and the dichloromethane phases were dried over $MgSO_4$. The crude product was purified by flash chromatography (petrol ether/dichloromethane 10:1) to produce **5a** (6.52 g, 74%) as a colorless solid. mp 240−242 °C. ^{1}H NMR (400 MHz, [D6]acetone, δ): 8.22 (dd, 2H, J = 8.3 and 0.5, CCHCHCCl), 7.47 (s, 2H, NCCHCCH_3), 7.38 (dd, 2H, J = 1.9 and 0.5, CCHCCl), 7.32 (dd, 2H, J = 8.3 and 1.9, CCHCHCCl), 2.56 (s, 6H, CH_3). ^{13}C NMR (400 MHz, CD_2Cl_2, δ): 142.3 (q), 141.1 (q), 135.3 (q), 132.3 (q), 127.6 (q), 127.0 (NCCHCCH_3), 121.7 (q), 121.6 (CCHCHCCl), 121.2 (CCHCHCCl), 110.5 (CCHCCl), 24.2 (CH_3). APCI positive (high resolution): $[M]^+$ calcd for $C_{20}H_{14}BrCl_2N$, 416.96812; found, 416.96700. Δ = 2.69 ppm.

9-(4-Bromo-3,5-dimethylphenyl)-3,6-dichloro-9H-carbazole **5b**. **5b** was prepared according to the preparation of **5a** using **3b** instead of **3a**. The reaction time was 19 h instead of 72 h. **5b** was obtained as a colorless solid (52%). mp 201−203 °C. ^{1}H NMR (400 MHz, CD_2Cl_2, δ): 8.06 (dd, 2H, J = 2.0 and 0.5, CC*H*CCl), 7.40 (dd, 2H, J = 8.8 and 2.0, CCHC*H*CCl), 7.31 (dd, 2H, J = 8.7 and 0.5, CC*H*CHCCl), 7.25 (s, 2H, NCC*H*CCH$_3$), 2.52 (s, 6H, CH_3). ^{13}C NMR (400 MHz, CD_2Cl_2, δ): 140.9 (q), 140.1 (q), 135.7 (q), 127.1 (CCH*C*HCCl), 126.7 (NC*C*HCCH$_3$), 126.0 (q), 123.8 (q), 120.5 (C*C*HCCl), 111.6 (C*C*HCHCCl), 24.2 (*C*H$_3$), *C*Br is missing. APCI positive (high resolution): $[M]^+$ calcd for $C_{20}H_{14}BrCl_2N$, 416.96812; found, 416.96829. Δ = 0.41 ppm.

2,7-Dichloro-9-(4-(diphenylmethyl)-phenyl)-9H-carbazole **6c**. **6c** was prepared according to the preparation of **5a** using **4b** instead of **4a** to give **6c** (82%) as a colorless solid. mp 203−205 °C. ^{1}H NMR (400 MHz, $CDCl_3$, δ): 7.98 (dd, 2H, J = 8.3 and 0.38), 7.44−7.34 (arom., 10H), 7.31−7.21 (arom., 8H), 5.68 (s, 1H). ^{13}C NMR (400 MHz, CD_2Cl_2, δ): 144.4 (q), 143.5 (q), 142.0 (q), 134.8 (q), 132.2 (q), 131.3 (*C*H), 129.6 (*C*H), 128.7 (*C*H), 126.87 (*C*H), 126.83 (*C*H), 121.5 (q), 121.2 (*C*H), 121.0 (*C*H), 110.3 (*C*H). EI-MS (high resolution, PI) *m/z*: calcd for $C_{31}H_{21}Cl_2N$, 477.10456; found, 477.10449. Δ = 0.14 ppm.

2,7-Dichloro-9-((4-dimesitylboryl)-3,5-dimethylphenyl)-9H-carbazole **6a**.[27] To a suspension of **5a** (370 mg, 883 μmol) in dry diethylether (10 mL), *t*-butyllithium (1.5 M in *n*-pentane, 1.17 mL, 1.76 mmol) was added at −68 °C. The reaction mixture was stirred for 3 h and then slowly added via cannula to a −68 °C cold solution of dimesitylboron fluoride (268 mg, 999 μmol) in dry diethylether (5 mL). The reaction mixture was allowed to warm up to room temperature overnight, diluted in dichloromethane, washed with water, and dried over $MgSO_4$. The crude product was purified by flash chromatography (petrol ether/dichloromethane 20:1) to give **6a** (285 mg, 55%) as a colorless solid. mp 265−267 °C. ^{1}H NMR (400 MHz, CD_2Cl_2, δ): 8.02 (d, 2H, J = 8.3, CC*H*CHCCl), 7.38 (d, 2H, J = 1.9, CC*H*CCl), 7.26 (dd, 2H, J = 8.3 and 1.9, CCHC*H*CCl), 7.07 (s, 2H, NCC*H*CCH$_3$), 6.84 (s, 2H, C*H*), 6.81 (s, 2H, C*H*), 2.30 (s, 6H, CH_3), 2.12 (s, 6H, CH_3), 2.11 (s, 6H, CH_3), 2.04 (s, 6H, CH_3). ^{13}C NMR (400 MHz, CD_2Cl_2, δ): 143.2 (q), 142.2 (q), 141.2 (q), 141.0 (q), 140.2 (q), 137.2 (q), 132.2 (q), 129.2 (*C*H), 129.1 (*C*H), 125.9 (NC*C*HCCH$_3$), 121.7 (q), 121.5 (C*C*HCHCCl), 121.1 (CCH*C*HCCl), 111.1 (q), 110.7 (C*C*HCCl), 108.9 (q), 23.1 (*C*H$_3$), 23.08 (*C*H$_3$), 23.02 (*C*H$_3$), 21.4 (*C*H$_3$). APCI positive (high resolution): $[M + H]^+$ calcd for $C_{38}H_{37}BCl_2N$, 587.24269; found, 587.24185. Δ = 1.43 ppm.

3,6-Dichloro-9-((4-dimesitylboryl)-3,5-dimethylphenyl)-9H-carbazole **6b**. **6b** was prepared according to the preparation of **6a** using **5b** instead of **5a**. The crude product was purified by precipitation from dichloromethane/methanol and recrystallization from ethylacetate to give **6b** (31%) as a colorless solid. mp 302−303 °C. ^{1}H NMR (600 MHz, CD_2Cl_2, δ): 8.05 (dd, 2H, J = 1.8 and 0.7, CC*H*CCl), 7.40 (dd, 2H, J = 8.7 and 1.8, CCHC*H*CCl), 7.38 (dd, 2H, J = 8.7 and 0.7, CC*H*CHCCl), 7.08 (s, 2H, NCC*H*CCH$_3$), 6.82 (s, 2H, C*H*), 6.80 (s, 2H, C*H*), 2.29 (s, 6H, CH_3), 2.10 (s, 6H, CH_3), 2.09 (s, 6H, CH_3), 2.03 (s, 6H, CH_3). ^{13}C NMR (600 MHz, CD_2Cl_2, δ): 147.8 (q), 143.9 (q), 142.9 (q), 141.1 (q), 140.9 (q), 140.2 (q), 139.9 (q), 137.5 (q), 129.09 (*C*H), 129.06 (*C*H), 126.9 (CCH*C*HCCl), 125.73 (NC*C*HCCH$_3$), 125.69 (q), 123.7 (q), 120.3 (C*C*HCCl), 111.8 (C*C*HCHCCl), 23.02 (*C*H$_3$), 23.00 (*C*H$_3$), 22.99 (*C*H$_3$), 21.3 (*C*H$_3$). APCI positive (high resolution): $[M]^+$ calcd for $C_{38}H_{36}BCl_2N$, 586.23487; found, 586.23460. Δ = 0.46 ppm.

Preparation of Polymers. Polymerization reactions were carried out according to the literature.[19]

Poly[9-((4-dimesitylboryl)-3,5-dimethylphenyl)-9H-carbazole]-2,7-diyl **P1**. Triphenylphosphine (109 mg, 414 μmol), zinc powder (153 mg, 2.34 mmol), 2,2′-bipyridyl (5.31 mg, 34.0 μmol), **6a** (421 mg, 716 μmol), and anhydrous nickel(II) chloride (4.38 mg, 33.8 μmol) were suspended in dry *N*,*N*-dimethylacetamide (1.15 mL) and stirred at 70 °C for 3 days. Then, 40 mL of HCl (10%)/methanol (1:5) were added to the gray-brown suspension, and it was stirred until all zinc powder had been reduced. The solid was filtered off, washed with water, and transferred to a Soxhlet apparatus, where it was washed with acetone for 24 h. Finally, it was dried under reduced pressure to give a pale-yellow solid (63%). Decomposition: 341 °C. ^{1}H NMR (400 MHz, $CDCl_3$, δ): 8.28−8.19, 8.18−8.14, 8.07−8.03, 7.70−7.50, 7.44−7.38, 7.20−7.13, 7.12−7.08, 6.83−6.68, 2.32−2.23, 2.14−2.05, 2.05−1.96. ^{13}C NMR (600 MHz, $CDCl_3$): could not be recorded because of low solubility. MALDI-MS *m/z*: calcd for $C_{228}H_{218}B_6N_6$, 3107.08; found, 3106.98 (Δ = 35 ppm); calcd for $C_{266}H_{254}B_7N_7$, 3624.59; found, 3624.68 (Δ = 23 ppm); calcd for $C_{304}H_{290}B_8N_8$, 4142.10; found, 4142.27 (Δ = 39 ppm); calcd for $C_{342}H_{326}B_9N_9$, 4659.61; found, 4659.81 (Δ = 41 ppm); calcd for $C_{380}H_{362}B_{10}N_{10}$, 5177.12; found, 5177.51 (Δ = 74 ppm); calcd for $C_{418}H_{398}B_{11}N_{11}$, 5694.63; found, 5694.61 (Δ = 4 ppm). GPC (in THF): M_w = 2300, M_n = 2100, PDI = 1.1; (in TCB):[49] M_w = 4000, M_n = 2300, PDI = 1.8;

Poly[9-((4-dimesitylboryl)-3,5-dimethylphenyl)-9H-carbazole]-3,6-diyl **P2**. **P2** was prepared according to the preparation of **P1** using monomer **6b**. Pale-yellow solid (53%). Decomposition: 324 °C. ^{1}H NMR (600 MHz, [D8]THF, δ): 8.9−8.1 (2H, C*H*), 8.0−7.6 (2H, C*H*), 7.6−7.3 (2H, C*H*), 7.3−7.0 (2H, C*H*), 6.8 (4H, C*H*), 2.3−2.2 (6H, CH_3), 2.2−1.9 (18H, CH_3). ^{13}C NMR (600 MHz, [D8]THF, δ): 147.5 (q), 144.8 (q), 143.5 (q), 141.6 (q), 141.4 (q), 141.1 (q), 140.5 (q), 139.8 (q), 135.3 (q), 129.8 (*C*H), 129.7 (*C*H), 126.3 (2C, *C*H), 125.5 (q), 119.6 (*C*H), 111.2 (*C*H), 22.3 (3C, *C*H$_3$), 20.4 (*C*H$_3$). MALDI-MS *m/z*: calcd for $C_{228}H_{218}B_6N_6$, 3107.08; found, 3106.99 (Δ = 29 ppm); calcd for $C_{266}H_{254}B_7N_7$, 3624.59; found, 3624.64 (Δ = 14 ppm); calcd for $C_{304}H_{290}B_8N_8$, 4142.10; found, 4142.09 (Δ = 2.4 ppm); calcd for $C_{342}H_{326}B_9N_9$, 4659.61; found, 4659.86 (Δ = 54 ppm); calcd for $C_{380}H_{362}B_{10}N_{10}$, 5177.12; found, 5177.29 (Δ = 33 ppm); calcd for $C_{418}H_{398}B_{11}N_{11}$,

5694.63; found, 5694.72 (Δ = 16 ppm); calcd for $C_{456}H_{434}B_{12}N_{12}$, 6212.14; found, 6212.50 (Δ = 58 ppm); calcd for $C_{494}H_{470}B_{13}N_{13}$, 6729.65; found, 6729.62 (Δ = 4.5 ppm); calcd for $C_{532}H_{506}B_{14}N_{14}$, 7247.16; found, 7247.47 (Δ = 43 ppm). GPC (in THF): M_w = 6000, M_n = 4900, PDI = 1.2;

Poly[9-(4-(diphenylmethyl)-phenyl)-9H-carbazole]-2,7-diyl **P3**. **P3** was prepared according to the preparation of **P1** using monomer **6c**. Yellow solid (52%). Decomposition: 335 °C. ^{1}H NMR (400 MHz, $CDCl_3$, δ): 8.21−8.0 (arom., 2H), 7.68−7.28 (arom., 12H), 7.23−7.17 (arom., 6H), 5.66−5.58 (benzylic, 1H). ^{13}C NMR (600 MHz, $CDCl_3$): could not be recorded because of low solubility; MALDI-MS *m/z*: calcd for $C_{93}H_{65}N_3$, 1223.52; found, 1223.49 (Δ = 24 ppm); calcd for $C_{124}H_{86}N_4$, 1630.68; found, 1630.69 (Δ = 4 ppm); calcd for $C_{155}H_{107}N_5$, 2037.85; found, 2037.92 (Δ = 35 ppm). GPC (in THF): M_w = 1900, M_n = 1700, PDI = 1.1;

Acknowledgment. We are grateful to Prof. K. Müllen and S. Seiwald of the MPI für Polymerforschung Mainz and K. Scherbaum of the Frauenhofer Institut für Silikatforschung Würzburg for preliminary GPC measurements of the polymers. We thank Prof. F. Würthner of the Universität Würzburg, Institut für Organische Chemie, for the ability to use the Absolute PL Quantum Yield Measurement System (Hamamatsu). We thank Prof. V. Dyakonov, Daniel Rauh, and Andreas Baumann of the Universität Würzburg, Fakultät für Physik and Astronomie, for assistance in constructing single-layer OLEDs. We thank the Deutsche Forschungsgemeinschaft for financial support.

References and Notes

(1) Morin, J.-F.; Leclerc, M.; Adès, D.; Siove, A. *Macromol. Rapid Commun.* **2005**, *26*, 761–778.
(2) Blouin, N.; Michaud, A.; Gendron, D.; Wakim, S.; Blair, E.; Neagu-Plesu, R.; Belletête, M.; Durocher, G.; Tao, Y.; Leclerc, M. *J. Am. Chem. Soc.* **2008**, *130*, 732–742.
(3) Paliulis, O.; Ostrauskaite, J.; Gaidelis, V.; Jankauskas, V.; Strohriegl, P. *Macromol. Chem. Phys.* **2003**, *204*, 1706–1712.
(4) Romero, D. B.; Schaer, M.; Leclerc, M.; Adès, D.; Siove, A.; Zuppiroli, L. *Synth. Met.* **1996**, *80*, 271–277.
(5) Stéphan, O.; Vial, J.-C. *Synth. Met.* **1999**, *106*, 115–119.
(6) Morin, J.-F.; Beaupré, S.; Leclerc, M.; Lévesque, I.; D'Iorio, M. *Appl. Phys. Lett.* **2002**, *80*, 341–343.
(7) Lmimouni, K.; Legrand, C.; Chapoton, A. *Synth. Met.* **1998**, *97*, 151–155.
(8) Tirapattur, S.; Belletête, M.; Drolet, N.; Leclerc, M.; Durocher, G. *Chem. Phys. Lett.* **2003**, *370*, 799–804.
(9) Morin, J.-F.; Leclerc, M. *Macromolecules* **2002**, *35*, 8413–8417.
(10) Iraqi, A.; Wataru, I. *Chem. Mater.* **2004**, *16*, 442–448.
(11) Sonntag, M.; Strohriegl, P. *Chem. Mater.* **2004**, *16*, 4736–4742.
(12) Zotti, G.; Schiavon, G.; Zecchin, S.; Morin, J.-F.; Leclerc, M. *Macromolecules* **2002**, *35*, 2122–2128.
(13) Doi, H.; Kinoshita, M.; Okumoto, K.; Shirota, Y. *Chem. Mater.* **2003**, *15*, 1080–1089.
(14) Jia, W.-L.; Bai, D.-R.; McCormick, T.; Liu, Q.-D.; Motala, M.; Wang, R.-Y.; Seward, C.; Tao, Y.; Wang, S. *Chem.—Eur. J.* **2004**, *10*, 994–1006.
(15) Iraqi, A.; Simmance, T. G.; Yi, H.; Stevenson, M.; Lidzey, D. G. *Chem. Mater.* **2006**, *18*, 5789–5797.
(16) Zhao, C.-H.; Wakamiya, A.; Inukai, Y.; Yamaguchi, S. *J. Am. Chem. Soc.* **2006**, *128*, 15934–15935.
(17) Wakamiya, A.; Mori, K.; Yamaguchi, S. *Angew. Chem., Int. Ed.* **2007**, *46*, 4273–4276.
(18) Elbing, M.; Bazan, G. C. *Angew. Chem., Int. Ed.* **2008**, *47*, 834–838.
(19) Morin, J.-F.; Leclerc, M. *Macromolecules* **2001**, *34*, 4680–4682.
(20) Ullmann, F.; Meyer, G. M.; Loewenthal, O.; Gilli, E. *Justus Liebigs Ann. Chem.* **1904**, *332*, 38–81.
(21) Hammann, W. C.; Schisla, R. M. *J. Chem. Eng. Data* **1972**, *17*, 112–115.
(22) Dierschke, F.; Grimsdale, A. C.; Müllen, K. *Synthesis* **2003**, *16*, 2470–2472.
(23) Cadogan, J. I. G.; Cameron-Wood, M.; Mackie, R. K.; Searle, R. J. G. *J. Chem. Soc.* **1965**, 4831–4837.
(24) Chmielewski, M. J.; Charon, M.; Jurczak, J. *Org. Lett.* **2004**, *6*, 3501–3504.
(25) Doyle, M. P.; Siegfried, B.; Dellaria, J. F. *J. Org. Chem.* **1977**, *42*, 2426–2431.
(26) de Groot, J. H.; Dillingham, K.; Deuring, H.; Haitjema, H. J.; van Beijma, F. J.; Hodd, K.; Norrby, S. *Biomacromolecules* **2001**, *2*, 1271–1278.
(27) Stahl, R.; Lambert, C.; Kaiser, C.; Wortmann, R.; Jakober, R. *Chem.—Eur. J.* **2006**, *12*, 23582370..
(28) Brook, A. G.; Gilman, H.; Miller, L. S. *J. Am. Chem. Soc.* **1953**, *75*, 4759–4765.
(29) Yamamoto, T.; Morita, A.; Miyazaki, Y.; Maruyama, T.; Wakayama, H.; Zhou, Z.-h.; Nakamura, Y.; Kanbara, T.; Sasaki, S.; Kubota, K. *Macromolecules* **1992**, *25*, 1214–1223.
(30) Fu, Y.; Bo, Z. *Macromol. Rapid Commun.* **2005**, *26*, 1704–1710.
(31) Wakim, S.; Blouin, N.; Gingras, E.; Tao, Y.; Leclerc, M. *Macromol. Rapid Commun.* **2007**, *28*, 1798–1803.
(32) Li, J.; Dierschke, F.; Wu, J.; Grimsdale, A. C.; Müllen, K. *J. Mater. Chem.* **2006**, *16*, 96–100.
(33) Zhang, Z.-B.; Fujiki, M.; Tang, H.-Z.; Motonaga, M.; Torimitsu, K. *Macromolecules* **2002**, *35*, 1988–1990.
(34) Iovu, M. C.; Sheina, E. E.; Gil, R. R.; McCullough, R. D. *Macromolecules* **2005**, *38*, 8649–8656.
(35) Ostrauskaite, J.; Strohriegl, P. *Macromol. Chem. Phys.* **2003**, *204*, 1713–1718.
(36) Yokozawa, T.; Adachi, I.; Miyakoshi, R.; Yokoyama, A. *High Perform. Polym.* **2007**, *19*, 684–699.
(37) The solution had to be filtered because there were a few undissolved particles visible. Therefore, the concentration is lower, and ε is even higher than calculated.
(38) Perkampus, H.-H. *UV-VIS Atlas of Organic Compounds*; VCH: Weinheim, Germany, 1992; p 532.
(39) Belletête, M.; Bouchard, J.; Leclerc, M.; Durocher, G. *Macromolecules* **2005**, *38*, 880–887.
(40) Strickler, S. J.; Berg, R. A. *J. Chem. Phys.* **1962**, *37*, 814–822.
(41) Siebrand, W. *J. Chem. Phys.* **1967**, *46*, 440–447.
(42) Iraqi, A.; Wataru, I. *J. Polym. Sci., Part A: Polym. Chem.* **2004**, *42*, 6041–6051.
(43) Kulasi, A.; Yi, H.; Iraqi, A. *J. Polym. Sci., Part A: Polym. Chem.* **2007**, *45*, 4957–4967.
(44) Iraqi, A.; Wataru, I. *Synth. Met.* **2001**, *119*, 159–160.
(45) Iraqi, A.; Pegington, R. C.; Simmance, T. G. *J. Polym. Sci., Part A: Polym. Chem.* **2006**, *44*, 3336–3342.
(46) The determination of the LUMO energies by the electrochemically measured HOMO energies and the optical excitation leads to energies that are too low because exciton binding energy (which is unknown) is not taken into account. Therefore, we refrain from presenting these optically estimated LUMO energies.
(47) Liu, R.; Xiong, Y.; Zeng, W.; Wu, Z.; Du, B.; Yang, W.; Sun, M.; Cao, Y. *Macromol. Chem. Phys.* **2007**, *208*, 1503–1509.
(48) Melluish, W. H. *J. Phys. Chem.* **1961**, *65*, 229–235.
(49) Measured by Max Planck Institute for Polymer Research, Mainz (Germany).

MA802232R